Energy & Environmental Science

ROYAL SOCIETY OF CHEMISTRY

PAPER

View Article Online
View Journal | View Issue

Cite this: *Energy Environ. Sci.*, 2023, **16**, 3040

Three-dimensional chiral networks of triboelectric nanogenerators inspired by metamaterial's structure†

Xianye Li,[ab] Liang Xu,*[ab] Pei Lin,*[ad] Xiaodan Yang,[ab] Huamei Wang,[ab] Huaifang Qin[ab] and Zhong Lin Wang*[ac]

Clusters of machinery units coupled tightly may emerge collective behavior and act like the metamaterial to tackle agitations from the environment. It is especially meaningful for exploiting water wave energy, which is a promising clean energy source with enormous reserves but a formidable challenge for traditional bulky generators. Here, a novel three-dimensional (3D) chiral network of triboelectric nanogenerators (TENGs) is designed for the first time to effectively harvest water wave energy based on this idea. Unlike traditional bulky and rigid machines, the 3D TENG network adopts a distributed architecture with chiral connections between unbalanced units, which imparts the network flexibility, hyper-elasticity in water, and wave-absorption behavior, similar to mechanical chiral metamaterials. The network can be configured to different scales and depths to harvest wave energy in all directions. A comprehensive energy harvesting system integrated with a power management circuit is constructed, with the stored energy enhanced by about 319 times. The novel 3D chiral network shows great potential for blue energy harvesting and self-powered systems based on TENGs, which can be more adaptive to severe ocean environments with flexible and distributed characteristics. This study also presents an insightful paradigm shift from mechanical metamaterial designs to energy harvesting networks, with similarities in mechanical wave energy absorption and conversion, inspiring novel energy harvesting systems and other strongly coupled machinery systems of multiple units based on metamaterials.

Received 1st April 2023,
Accepted 19th May 2023

DOI: 10.1039/d3ee01035j

rsc.li/ees

Broader context

Triboelectric nanogenerators (TENGs) provide new opportunities to develop energy harvesting systems of novel forms, especially for water wave energy, which is a huge clean energy reserve in the ocean, yet with formidable challenges to harvest by traditional technologies. Herein, we developed a network of multiple TENG units based on the metamaterial structure, presenting wave absorption behavior, and other exotic characteristics under wave excitations are also expected to achieve boosted performance for solving the long-standing challenge of effective wave energy harvesting. The network represents an inspiring form of metamaterial using machinery units to tackle waves. Moreover, this study builds up a new architecture of distributed unit clusters instead of monolithic machines for certain tasks like many biological systems, such as ant colonies, with strong coupling among units and environment, paving the way to novel machinery clusters with performance unreachable by traditional machines.

Introduction

As a manmade material with underlying geometrical structures, the metamaterial provides new design freedoms and unconventional properties for manipulating electromagnetic waves, realizing exotic features, such as negative phase velocities and invisibility cloaking.[1,2] Recently, the idea is successfully applied to acoustics and mechanics, showing its adaptability for manipulating waves governed by other disciplines.[3–7] Therefore, it is reasonable to anticipate a machinery counterpart that is constituted by multiple distributed small units and interconnected according to the metamaterial structure. Such machinery

[a] *Beijing Institute of Nanoenergy and Nanosystems, Chinese Academy of Sciences, Beijing, 101400, P. R. China. E-mail: xuliang@binn.cas.cn*
[b] *School of Nanoscience and Technology, University of Chinese Academy of Sciences, Beijing, 100049, P. R. China*
[c] *Georgia Institute of Technology, Atlanta, Georgia, 30332-0245, USA. E-mail: zlwang@gatech.edu*
[d] *Key Laboratory of Materials Physics of Ministry of Education, School of Physics and Microelectronics, Zhengzhou University, Zhengzhou, 450001, P. R. China. E-mail: linpei@zzu.edu.cn*

† Electronic supplementary information (ESI) available. See DOI: https://doi.org/10.1039/d3ee01035j

systems can further enrich the concept of metamaterials and provide a new paradigm for designing machines that involve tight coupling with environmental mechanical agitations. Extraordinary characteristics and emerging behavior that are unreachable for conventional bulky machines can be expected, which is especially meaningful for solving traditional challenges in related areas.

As one of the huge renewable and clean energy reserves in the ocean,[8,9] the utilization of wave energy is considered a promising approach to optimize energy structure globally and achieve carbon neutrality[10] due to its wide distribution, easy accessibility, and large reserves, which can reach over 2 TW (1 TW = 10^{12} W) around the coastline globally under an estimation.[11,12] Nevertheless, features of low frequency, irregularity, wide distribution, and small power density greatly hinder the effective harnessing of such energy, despite several decades of efforts worldwide to design huge and bulky equipment based on electromagnetic generators for wave energy harvesting, which are usually costly and can be fragile in the severe ocean environment.[8,9,13] Considering it concerns tackling distributed waves, a machinery system consisting of multiple devices according to the metamaterial structure may provide an effective solution to this formidable challenge. Actually, similar systems as robot swarms have already been proposed to mimic the collective behavior of biological colonies in nature, such as ants and bees, for fulfilling certain tasks.[14–17] However, in such robot systems, the units are usually loosely and locally interacted. The system based on the metamaterial represents another paradigm of clusters of machinery units for certain tasks, with a strong coupling of energy exchange or force interaction among units and coherent motion behavior to respond to environment agitations.

The concept can be realized by adopting the triboelectric nanogenerator (TENG) as the element device, which can harvest mechanical energy in the environment with high flexibility in size and structure.[18–21] TENG converts mechanical energy into electric power through triboelectrification and electrostatic induction.[20,22–24] Since its invention in 2012, it has been proven to be very effective in harvesting environment mechanical energy, such as vibration, wind, rain, water wave, and so on, with the merits of low cost, easy fabrication, and rich material and structure choices.[24–33] The attempts to harvest wave energy by TENGs have realized several prototypes of structural designs, performance optimizations, and even simple networks,[12,19,34–38] yet with unsatisfactory performance.

In this work, inspired by the structure of mechanical metamaterials, a novel three-dimensional (3D) chiral network of triboelectric nanogenerators is designed for the first time to effectively harvest water wave energy. Unlike traditional bulky and rigid machines, the 3D TENG network adopts a distributed architecture with chiral connections between unbalanced units, which imparts the network flexibility, hyper-elasticity in water, and wave-absorption behavior, similar to mechanical chiral metamaterials. The network can be configured to different scales and depths to harvest wave energy in all directions. Networks with different configurations are studied and the dependence of output on the frequency and height of waves is investigated in detail. A comprehensive energy harvesting system integrated with a power management circuit is constructed, with the stored energy enhanced by about 319 times, and a self-powered sensing and signal transmission system is demonstrated. The novel 3D chiral network shows great potential for ocean blue energy harvesting and self-powered systems based on TENGs, which can be more adaptive to severe ocean environments with flexible and distributed characteristics. The work also presents an insightful paradigm shift from mechanical metamaterial designs to energy harvesting networks, with similarities in mechanical wave energy absorption and conversion, inspiring novel energy harvesting systems and other strongly coupled machinery systems of multiple units based on metamaterials.

Results and discussion

Concept of the 3D chiral TENG network

The concept of the 3D chiral TENG network is depicted in Fig. 1(A), which presents distributed architectures evolved from monolithic machines. Similar to the robot swarms, the function of a traditional bulky machine can be realized by a distributed cluster of small devices, which are further interconnected into a network with strong coupling, and the structure of mechanical metamaterials is referred to for achieving desired dynamic behavior in wave agitations. Consequently, a 3D chiral TENG network is constructed, which extends underwater from the water surface and is composed of floats, chiral units, and connecting ligaments between units. In detail, the network consists of several layers of chiral units. Along the vertical direction, adjacent units are asymmetrically connected by two flexible ligaments to form a long chiral chain, and in the horizontal direction, units at the same layer of different chains are connected by another two flexible ligaments to synchronize the motion in each layer. All the binding points of the ligaments with the units are at the horizontal central plane of the unit. Typically, three chains are involved to form a tubular-structured module that can be regarded as rolled from a plane. The chiral unit is fabricated by attaching a semispherical mass shell to a TENG. The floats at the top layer can keep the network near the water surface where wave energy is distributed. Upon the agitation of water waves or water current, chiral units can be actuated to rock periodically through chiral connections. Moreover, the motion and agitation energy can be transmitted along the chains to excite every unit even when the network is partly disturbed. Such motion and energy transmission capabilities are crucial for deploying large-scale energy harvesting networks or networks deep under the water surface.

The 3D chiral network is inspired by the structure and response behavior of the mechanical chiral metamaterial shown in Fig. 1(A). A basic unit of the structure consists of an annulus node and four ligaments, which connect annuluses in adjacent units. As the extended line of the ligament does not pass the center of the annulus, the unit only has rotational symmetry without centrosymmetry; thus it is chiral with no

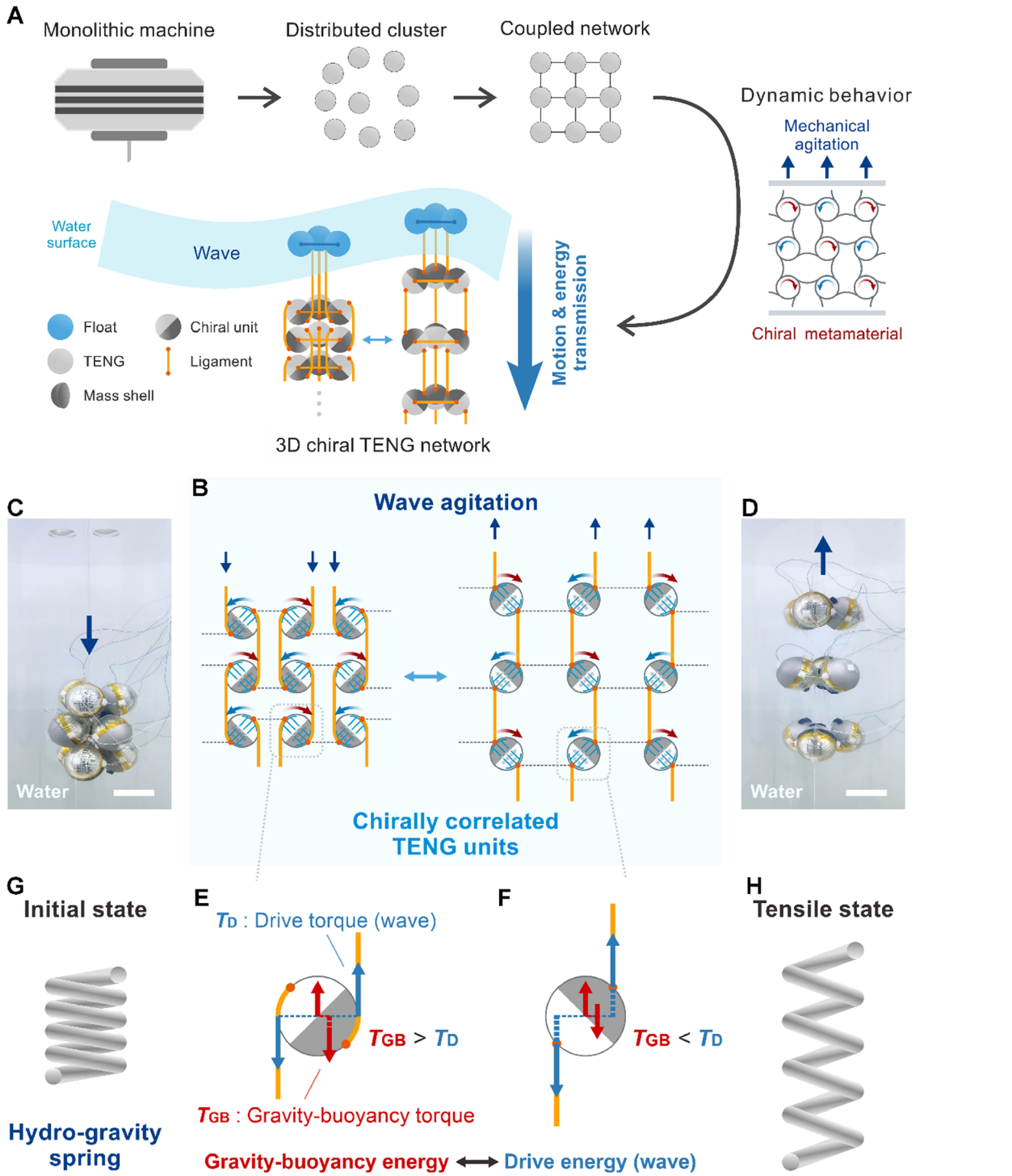

Fig. 1 Concept of the 3D chiral TENG network. (A) Schematic illustration of the 3D chiral TENG network. (B) The working mechanism of the chiral TENG network. (C and D) Photographs of the 3D chiral TENG network in water with the initial state (C) and tensile state (D). Scale bar, 8 cm. (E) and (F) Force–torque coupling at a single chiral unit in the initial state (E) and tensile state (F). (G) and (H) Schematics of an analogical hydro-gravity spring in the initial state (G) and tensile state (H).

superimposition on its mirror image.[39,40] When mechanically pushed or pulled, the chiral metamaterial behaves as flexing of the ligaments and rotating of the annulus nodes, exhibiting capabilities of transforming translational agitation into rotational motion of the units. The material can further exhibit characteristics of mechanical wave absorption or manipulation when dynamically excited by mechanical waves based on certain optimization.[3,5,7] It can guide the design of TENG networks with exceptional properties which aim to be agitated by mechanical water waves and "dissipates" the energy into

electricity. Based on the force–torque coupling of the chiral structure, the network can transform the agitation of water waves into rotational motion of TENG units, which is adaptive to most high-performance TENG structures,[28,41,42] and it can also accelerate the motion like a pinion and rack mechanism.

The detailed working mechanism of the chiral TENG network is presented in Fig. 1(B)–(H). To intuitively illustrate the process of motion, the typical 3D chiral network module is unfolded onto a 2D plane with neglected horizontal ligaments. Fig. 1(B) clearly demonstrates how the chirally correlated TENG units are agitated to rotate by the fluctuation of water waves due to symmetry breaking, which is verified by the fabricated network experimented in a water environment, as shown in Fig. 1(C) and (D). The force–torque coupling at a single unit is shown in Fig. 1(E) and (F). Two sets of forces on the unit impose two torques in opposite directions, taking the center of the unit as the pole. First, the buoyancy of the unit acts at the center of the TENG, while the gravity of the chiral unit acts at an offset point due to the unbalanced mass shell. Thus, they impose a so-called gravity–buoyancy torque ($\boldsymbol{T}_{\mathbf{GB}}$) on the chiral unit. The pull of waves can produce tension on the upper and lower ligaments, imposing another two forces, resulting in another torque named the drive torque ($\boldsymbol{T}_{\mathbf{D}}$). With the variation of the drive torque underwater wave fluctuation, the chiral units are driven to roll back and forth, accompanied by the energy transformation between gravity–buoyancy energy and drive energy with part of the energy absorbed by the TENG units for generating electricity. Considering the gravity–buoyancy energy is potential energy, the behavior of the chiral chain is very similar to a spring (Fig. 1(G), (H) and Movie S1, ESI†), which can be regarded as a hydro-gravity spring with hyperelasticity.

Structure, working principle, and electrical characterization of the network unit

To demonstrate the energy harvesting performance of the network, a typical TENG structure with multilayer electrodes and intercalated pellets were used.[38] However, it should be emphasized that the 3D networking design is not limited to such a TENG structure. As shown in Fig. 2(A), the chiral unit features polytetrafluoroethylene (PTFE) pellets and a pair of multilayer electrodes inside a spherical shell, and the hemispherical mass shell is attached to one side of the spherical shell corresponding to one of the electrodes. The electrodes were fabricated by adhering Al layers on polyethylene terephthalate (PET) substrates. Fig. 2(B) shows the photograph of the as-fabricated TENG chiral unit. More details are described in the Experimental Section. The TENG units typically work in a rocking mode with a rocking angle θ as the motion amplitude, as shown in Fig. 2(C).

The working mechanism of the TENG is depicted in Fig. 2(D). The rocking motion of the device changes the gravitational potential energy (E_p) landscape for the pellets with shifting energy wells (Fig. 2(D)), inducing the pellets to roll between two electrodes. Upon rolling on the Al electrodes, the surface of the PTFE pellets is negatively electrified owing to a higher affinity for electrons.[43] Correspondingly, Al electrodes are positively electrified. PTFE pellets with negative charges shuttle between the two electrodes, accompanied by the flowing of free electrons through the external circuit due to electrostatic induction. Consequently, mechanical energy is converted into electricity.

For characterizing the performance of the typical TENG unit, harmonic agitations with rocking angle θ and frequency f were exerted on the TENG by a linear motor. The short-circuit transferred charges Q_{SC} and current I_{SC} rise with the increase of θ and saturate to peak values of 0.54 μC and 4.34 μA respectively, under an agitation frequency of 1.5 Hz (Fig. 2(E) and (F)). Similarly, the dependence of electrical output on the agitation frequency was studied, as shown in Fig. S1 (ESI†). Fig. 2(G) demonstrates the capability of the TENG to charge commercial capacitors after rectification under the agitation of $\theta = 135^\circ$ and $f = 1.5$ Hz. The power output of a single TENG with different resistive loads was also tested. As presented in Fig. 2(H), a maximum peak power of 7.88 mW and average power of 2.18 mW reached around 1 GΩ.

To scale up the output with multiple TENGs as a network, the dependence of the electric output on the number of units was investigated. Nine TENG units were fabricated and tested individually first under the agitation of $\theta = 90^\circ$ and $f = 1.5$ Hz, and the units exhibited uniform electric output, as shown in Fig. S2 (ESI†). Then, the TENGs were tested in parallel connection while being maintained in the same phase. The transferred charges show a linear relationship with the number of units, ascending to 3.7 μC for 9 units (Fig. 2(I)), and the rectified short-circuit current presented the same tendency to 27.77 μA (Fig. 2(J)).

Structure and characteristics of the 3D chiral TENG network

Based on the connection mode of the chiral units at adjacent layers, the chiral chain can be classified into three different types, namely the serial, parallel, and hybrid types, as shown in Fig. 3(A)–(C). The chiral units of the two adjacent layers in the serial type are mirror images of each other, while they are replicas in the parallel type. The hybrid type is the hybridization of the two. Due to the unbalanced design of the units, the side with the mass shell is much heavier than the other side, and thus it tends to go down to achieve a minimum-energy state, inducing the rolling motion of the units. If a drive force acts, the chain will be pulled off the minimum-energy state with motion and energy transmission along the chain. In this situation, the mass shell side will go upward with a reversed rolling motion for each unit, unfolding the chiral chain, as shown in Fig. 3(A)–(C). It should be noticed that the rotating directions of the units in serial and parallel chiral chains are different.

To deeply understand the behavior of the chiral chain, the force on chiral units along the vertical direction was analyzed. Here, a simplified model was adopted where the damping of water was neglected and the ligament was assumed vertical except for the part wound on the TENG surface. The motion of the chain was assumed to be quasi-static, thus each unit was nearly in force balance. As shown in Fig. 3(D), for the unit in the

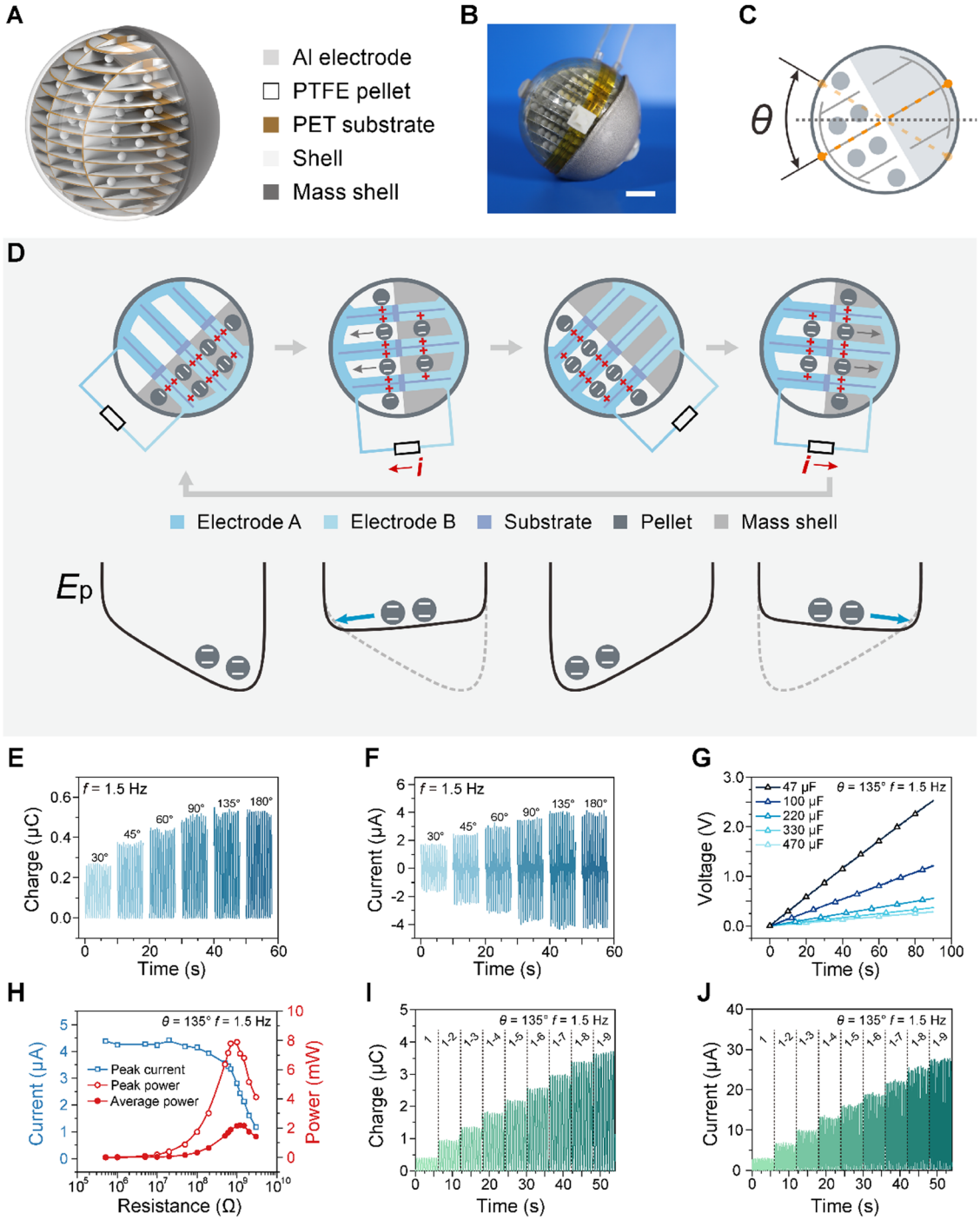

Fig. 2 Structure, working principle, and electrical characterization of the network unit. (A) Schematic structure of the chiral unit. (B) Photograph of the as-fabricated chiral unit. Scale bar, 2 cm. (C) Schematic diagram of the rocking mode. (D) The working mechanism of the TENG. (E) and (F) Dependence of transferred charges (E) and short-circuit current (F) on the rocking angle. (G) Charging performance of the TENG to various capacitors. (H) Peak current, peak power, and average power of the TENG under different loads. (I) and (J) Dependence of rectified transferred charges (I) and short-circuit current (J) on the number of units.

serial chain, the involved forces are forces exerted by the upper and lower ligaments ($\boldsymbol{F}_{\mathbf{U}}$ and $\boldsymbol{F}_{\mathbf{L}}$), the gravity of the unit without the pellets ($\boldsymbol{G}_{\mathbf{M}}$), gravity of the pellets ($\boldsymbol{G}_{\mathbf{P}}$), and buoyancy of the unit ($\boldsymbol{F}_{\mathbf{f}}$). The $\boldsymbol{G}_{\mathbf{M}}$ does not act on the center of the spherical shell due to the mass shell, while the $\boldsymbol{F}_{\mathbf{f}}$ is regarded to act on the center by neglecting the volume of the mass shell. Considering the force balance, the forces are related by the following equation:

$$\boldsymbol{F}_{\mathbf{U}} + \boldsymbol{F}_{\mathbf{L}} + \boldsymbol{G}_{\mathbf{M}} + \boldsymbol{G}_{\mathbf{P}} + \boldsymbol{F}_{\mathbf{f}} = 0 \quad (1)$$

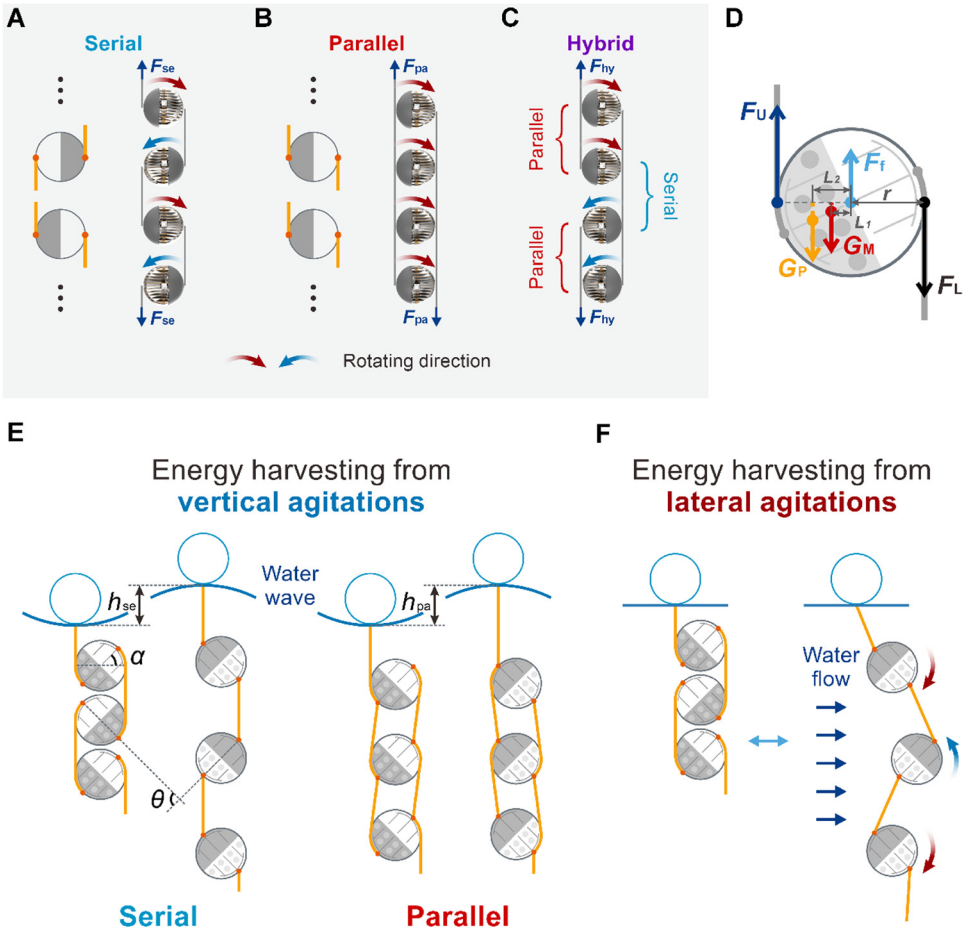

Fig. 3 Structure and characteristics of the 3D chiral TENG network. (A)–(C) Serial (A), parallel (B), and hybrid (C) types of chiral chains. (D) Force analysis along the vertical direction of the chiral unit in the serial chain. (E) and (F) Schematic illustrations of energy harvesting from vertical agitations (E) and lateral agitations (F).

Thus, if the gravity is equal to the buoyancy (which can be tuned in device fabrication), the forces in the upper and lower ligaments are the same:

$$\boldsymbol{F}_{\mathbf{U}} = \boldsymbol{F}_{\mathbf{L}} \tag{2}$$

and so are the forces in the ligaments throughout the chiral chain (Fig. S3A, ESI†), which ensures that the rocking motion amplitude for all units in the serial chain can be equal. The gravity–buoyancy torque ($\boldsymbol{T}_{\mathbf{GB}}$) and the drive torque ($\boldsymbol{T}_{\mathbf{D}}$) are in opposite directions and can be calculated as follows when taking the center of the spherical shell as the pole:

$$|\boldsymbol{T}_{\mathbf{D}}| = r|\boldsymbol{F}_{\mathbf{U}}| + r|\boldsymbol{F}_{\mathbf{L}}| \tag{3}$$

$$|\boldsymbol{T}_{\mathbf{GB}}| = L_1|\boldsymbol{G}_{\mathbf{M}}| + L_2|\boldsymbol{G}_{\mathbf{P}}| + L_3|\boldsymbol{F}_{\mathbf{f}}| = L_1|\boldsymbol{G}_{\mathbf{M}}| + L_2|\boldsymbol{G}_{\mathbf{P}}| \tag{4}$$

where r is the radius of the spherical shell, and L_1, L_2, and L_3 are corresponding force arms. Generally, L_1 is a function of the rocking angle θ; L_2 will change with the motion of the pellets and the rocking angle θ; L_3 is zero. Considering the force balance:

$$|\boldsymbol{T}_{\mathbf{D}}| = |\boldsymbol{T}_{\mathbf{GB}}| \tag{5}$$

Based on eqn (2)–(5), for achieving a quasi-static motion, the driving force for the serial chain $\boldsymbol{F}_{\mathbf{se}}$ should be:

$$|\boldsymbol{F}_{\mathbf{se}}| = |\boldsymbol{F}_{\mathbf{U}}| = \frac{L_1|\boldsymbol{G}_{\mathbf{M}}| + L_2|\boldsymbol{G}_{\mathbf{P}}|}{2r} \tag{6}$$

For the parallel chain, the force analysis is shown in Fig. S3B (ESI†). There are typically extra forces $\boldsymbol{F'}_{\mathbf{U}}$ from another upper ligament and $\boldsymbol{F'}_{\mathbf{L}}$ from another lower ligament, thus the forces are superposed as shown in Fig. S3C (ESI†). When the rocking angle is small, due to that the force arms of $\boldsymbol{F'}_{\mathbf{U}}$, $\boldsymbol{F'}_{\mathbf{L}}$ are very close to those of $\boldsymbol{F}_{\mathbf{U}}$, $\boldsymbol{F}_{\mathbf{L}}$, for achieving a quasi-static motion, the driving force of the parallel chain $\boldsymbol{F}_{\mathbf{pa}}$ should be:

$$|\boldsymbol{F}_{\mathbf{pa}}| = n|\boldsymbol{F}_{\mathbf{se}}| \tag{7}$$

assuming that the rocking angle of each unit is the same as the serial case, and n is the number of units in the chain.

The relationship between the wave height and rocking angle of each unit was also theoretically analyzed, as shown in Fig. 3(E). As discussed above, the chain will enter a minimum-energy state without agitations, and units of adjacent layers will roll until contacting each other in the serial chain, corresponding to an initial angle α (in radians), as shown in Fig. 3(E), which can

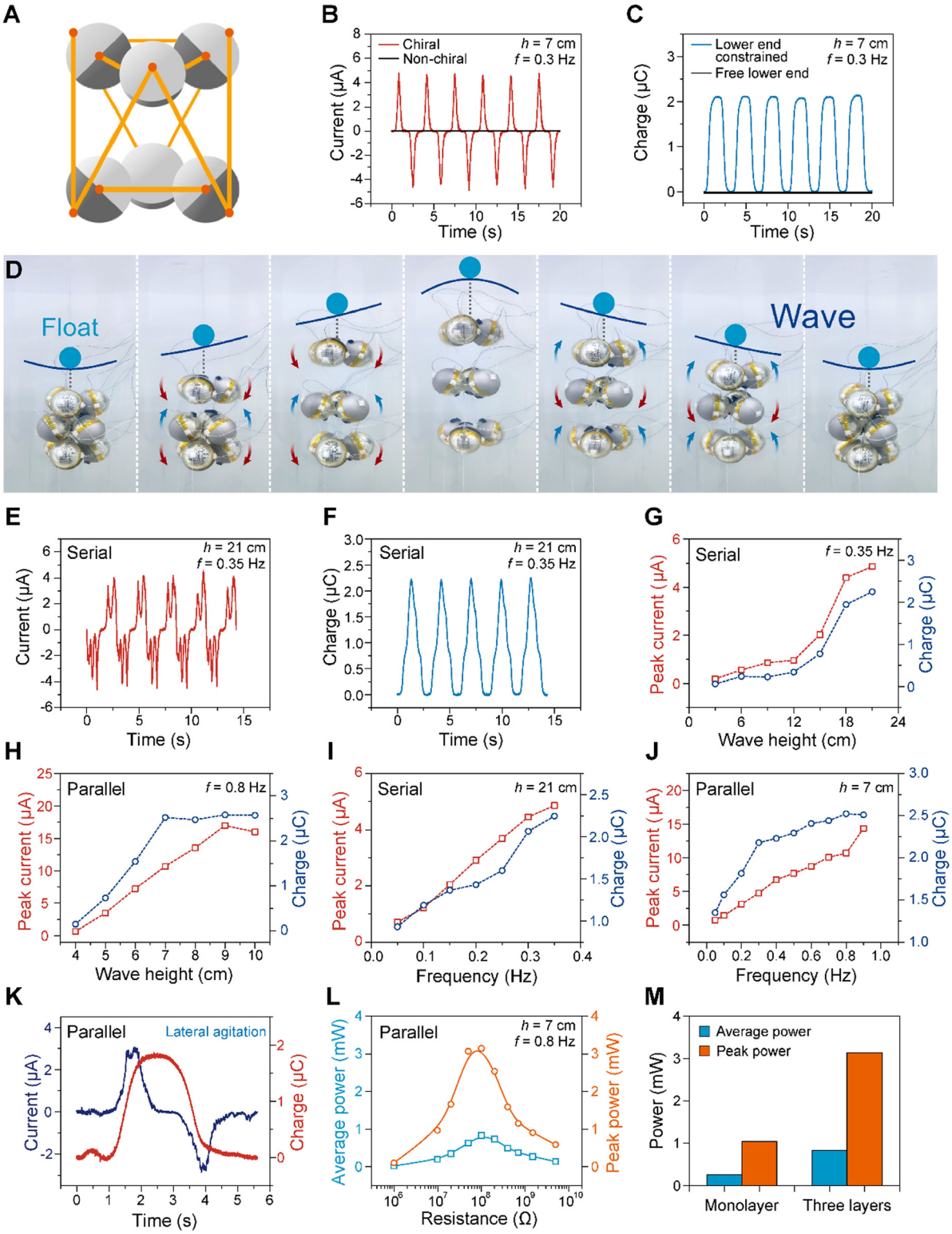

Fig. 4 Performance of the chiral network for wave energy harvesting. (A) Schematic structure of the shifted network. (B) Short-circuit current of the chiral and non-chiral networks. (C) Transferred charges of the network with different constraint states of the lower end. (D) Motion process of the serial network under undulating agitations in water. (E) and (F) Short-circuit current (E) and transferred charges (F) of the serial network. (G) and (H) Dependence of peak current and transferred charges of the serial network (G) and parallel network (H) on the wave height. (I) and (J) Dependence of peak current and transferred charges of the serial network (I) and parallel network (J) on the agitation frequency. (K) The output of the parallel network under the lateral agitation in one period. (L) Dependence of the output power of the parallel network on resistive loads. (M) Power comparison between networks of monolayer and three layers.

be adjusted by the length of the ligament and the radius of the spherical shell. On the other hand, with the designed initial angle α and the radius of the shell, the length of the ligament can be theoretically determined. Based on simple geometry, for the serial chain, the wave height h_{se} and rocking angle θ (in radians) are related by:

$$h_{se} = \begin{cases} 2nr\theta, & \theta \le \alpha \\ 2nr(\alpha + \sin(\theta - \alpha)), & \theta > \alpha \end{cases} \quad (8)$$

The height is the superposition of the ligament elongations of n units in the chain. For the parallel case, each unit rocks synchronously. If the same initial angle α is adopted and angles α and θ are small enough, the wave height h_{pa} and rocking angle θ can be approximately related by:

$$h_{pa} = \begin{cases} 2r\theta, & \theta \le \alpha \\ 2r(\alpha + \sin(\theta - \alpha)), & \theta > \alpha \end{cases} \quad (9)$$

Thus, in the above-mentioned conditions,

$$h_{pa} = \frac{1}{n} h_{se} \quad (10)$$

According to eqn (7) and (10), it is clear that to drive a chiral chain, a smaller force and larger wave height are needed for the serial type, and a larger force and smaller wave height are needed for the parallel type. The hybrid type will compromise the features of the above two types. Although in practical situations, the network can be away from the quasi-static state with deviations from such theoretical results, they are still meaningful as simple references for the network design.

Besides harvesting energy from vertical agitations, as shown in Fig. 3(E), lateral agitations of underwater flow also can actuate the chiral chain, as shown in Fig. 3(F). The water flow will push the chain away from the minimum-energy state, inducing the units to roll with the unfolding of the chiral structure and then restore, similar to the situation induced by the water waves. The water flow energy is absorbed by the structure and converted into electricity. This indicates that the 3D chiral network is capable of harvesting energy from agitations in all directions, greatly enhancing the omnidirectional performance of TENGs.

Performance of the chiral network for wave energy harvesting

The chiral chains are typically connected into a tubular structure as a network module (Fig. S4, ESI†). Here, nine units are fabricated and organized into three chains in serial or parallel type to characterize the performance of the 3D chiral network in a water tank (saline water with 3.5% salinity, for simulating real sea water). To enhance the stability along the horizontal direction, adjacent layers are shifted by 60° with modified ligament connections in practical networks, as shown in Fig. 4(A) and Fig. S5 (ESI†), which can ensure a more stable stacking state when folded due to smaller energy. Meanwhile, to make sure the serial unit can work in the most efficient rocking angles at limited wave heights, limit blocks are designed on the units, which allows the chiral unit to rotate about 90 degrees, as shown in Fig. S6 (ESI†).

The outputs of the chiral and non-chiral cases are compared first. In the non-chiral case, the ligaments along the vertical direction connect the units *via* the top and bottom points of each unit. As shown in Fig. 4(B), it is clear that chirality is crucial for the coupling of wave motion and TENG agitation. The short-circuit current of the parallel network reaches 4.87 μA, and without the chirality in the network, there is almost no output due to weak coupling. It should be noted that since the rocking motions of all units in the network module are at the same pace, their outputs can be directly connected together and superimposed without rectification, thus lowering the complexity of the system if a large number of units are involved.

The constraint at the lower end is also important for the network. Fig. 4(C) shows that the output of the parallel network with the lower end constrained is significantly better than the one with the free lower end, and the transferred charges of the former achieved about 2.14 μC. This can be attributed to that the driving force is not able to stretch the chiral chain with a free lower end, just like a non-fixed spring. Generally, the lower end can be connected to a damper or the water bottom, as shown in Fig. S7 (ESI†).

The motion process of the chiral network with the lower end constrained is shown in Fig. 4(D) and Movie S1 (ESI†). Upon undulating agitations, the serial network can be periodically unfolded and restored like a spring, accompanying coupled rocking motion of TENG units. Here, a linear motor is adopted for simulating the wave agitation and imposes an undulating displacement on the float at the water surface to precisely control the agitation condition, and the method is validated by a real wave experiment as shown in Movie S2 (ESI†). Since the initial state of the network is the most stable state with the lowest potential energy, any deformation of the network under external disturbances and agitations will restore to the initial state by itself (Fig. S8 and Movie S3, ESI†). This also implies that the structure can be very stable and robust even in complex ocean environments although flexible. The periodical movement of the parallel network under undulating agitations is shown in Fig. S9 (ESI†).

The output performance of the 3D chiral TENG network was further comprehensively characterized in the water tank. The short-circuit current of the serial network is 4.62 μA (Fig. 4(E)) and the charge output is 2.25 μC (Fig. 4(F)), at an agitation of h = 21 cm and f = 0.35 Hz, and the enlarged curves in one cycle are shown in Fig. S10 (ESI†). The short-circuit current and transferred charges of the parallel network reach 10.69 μA and 2.52 μC at h = 7 cm and f = 0.8 Hz, as shown in Fig. S11 (ESI†). The wide current peak is attributed to the concerted movement of the chiral units.

The dependence of the output performance on the wave height is studied, as shown in Fig. 4(G) and (H). For the serial network, at a low frequency of 0.35 Hz, the values of the peak current and transferred charges show similar growth trends with the increase of wave height from 3 to 21 cm. The serial

network is completely agitated at h = 21 cm and f = 0.35 Hz (Fig. 4(G)). Fig. 4(H) demonstrates the relationship between output and wave height for the parallel network at f = 0.8 Hz. The transferred charges were saturated at h = 7 cm. The above results demonstrate that a multiplied wave height is required for fully agitating the serial network compared with the parallel network, consistent with the theoretical results. Moreover, the dependence of output performance on the frequency is demonstrated in Fig. 4(I) and (J). Both outputs of the serial and parallel networks exhibit enhancing trends with increasing agitation frequencies.

Besides the vertical agitation discussed above, 3D chiral networks can also respond to lateral agitations. The movement and output of the parallel network under the lateral agitation in one period are shown in Fig. S12 (ESI†) and Fig. 4(K), respectively. A current of 3.06 μA and charges of 1.87 μC are achieved with lateral water disturbance. The movement and output of the serial network under lateral agitations are presented in Fig. S13 and S14 (ESI†), respectively. The power output under various resistive loads was also measured as shown in Fig. 4(L). Maximum peak power of 3.14 mW and average power of 0.82 mW were achieved with a resistive load of 100 MΩ at 0.8 Hz. The corresponding peak current and load voltage are shown in Fig. S15 (ESI†). It should be emphasized that the 3D chiral network structure is applicable for most high-performance TENG units, and the output power of the network will be consistent with the power of the TENG unit itself. The average power output here also represents the state-of-art performance under low-frequency and low-amplitude agitations, which are much closer to real ocean wave conditions, although the peak value that represents an instantaneous output can usually be very high. To study the power enhancement with multiple layers in 3D networks, the output performance of a chiral monolayer was measured, as presented in Fig. S16 (ESI†). The highest peak power is 1.04 mW, approximately one-third of the 3D network with three layers, as shown in Fig. 4(M), which clearly indicates that the output power of the network can be roughly linearly enhanced by increasing layers underwater for certain occupied ocean surface area, allowing much larger power densities.

Power management for the chiral network

Due to the mismatch of the high internal impedance of the TENG with most electrical devices, power management is required for applications that can also transform the alternating current into stable direct-current output.[44] As shown in Fig. 5(A), a power management circuit (PMC) based on the buck module was adopted here, which can be divided into three parts including rectification, buck, and regulation.[45,46] The energy harvested by the 3D chiral TENG network flows to C_{in} (100 pF) through a full-wave rectification circuit consisting of four high-voltage diodes (2CL72). The voltage control switch in the buck part is composed of a transient-voltage suppressor (TVS, P6KE440A) D_1 and a silicon-controlled rectifier (SCR, EC103M1). The positive pole of D_1 is connected to the gate of SCR and a shunt resistor can be considered according to the leakage current of D_1. The rest of the buck circuit consists of an inductor L (1 mH), a capacitor C_{out} and an ultrafast diode D_2 (MUR460). As C_{in} is charged to a voltage greater than the clamp voltage of D_1, the current surge through D_1 triggers SCR to conduct until the energy stored in C_{in} flows into the inductor. In the next phase, the current oscillates through the loop of L, C_{out}, and D_2, and the voltage on C_{out} will gradually increase for powering electronics. To meet the voltage requirement of electrical loads, a voltage regulator (LTC3588-1) is applied to stabilize the output voltage U_O before the load. Moreover, the voltage after the switch U_S can also be applied directly for powering some electronics, which require high instantaneous power, and the switch allows maximizing the energy output in one cycle.[47]

A comprehensive energy harvesting system integrated with the power management circuit was constructed and characterized, based on the parallel network agitated at h = 7 cm and f = 0.8 Hz unless otherwise specified. Firstly, the output after the switch was tested, as shown in Fig. 5(B)–(D). Fig. 5(B) presents that a high instantaneous peak current of 0.38 A can be generated by U_S with a 500 Ω resistor R,[27,29,48] and the duration of the peak current is about 4 μS, as shown in Fig. 5(C). Furthermore, the dependence of the instantaneous current and power on different resistive loads was tested. Maximum instantaneous peak power of 76.4 W was attained with a resistor of 500 Ω (Fig. 5(D)). Considering that each chiral TENG chain occupies a sea area of about 5.026×10^{-3} m^2, an area peak power density of 5066 W m^{-2} was calculated. The volume peak power density was 31 665 W m^{-3}. This indicates that with a switch circuit, an exceptionally high power output can be obtained. Although the power is instantaneous with a short duration of energy release, it is still meaningful for some electronics requiring instantaneous high power.[29] At the same time, the matched impedance is obviously reduced compared to outputting directly. For another output mode based on C_{out}, Fig. 5(E) compares the charging rates with and without power management, both using a capacitor of 1 mF. With power management, the rising rate of the stored energy in the capacitor is greatly enhanced by about 319 times.[45]

Application demonstrations of the chiral network

The 3D chiral TENG network as a TENG cluster is expected to be constituted in a hierarchical structure with different scales and depths for various applications. Fig. 6(A) demonstrates an exciting prospect of future application systems based on a large-scale 3D chiral TENG network as a marine power station. The TENG network is composed of several sub-networks, which assemble into an array of tubular modules together. A power management module gathering the harvested energy from each sub-network can distribute the electricity for different applications. A wide variety of devices and marine engineering are envisioned to be powered, such as underwater robots, wireless sensor networks, ocean buoys, offshore platforms, and fish farms. The electricity can also be transmitted to islands, and power grids on the mainland. Factories for seawater desalination and hydrogen production may use such

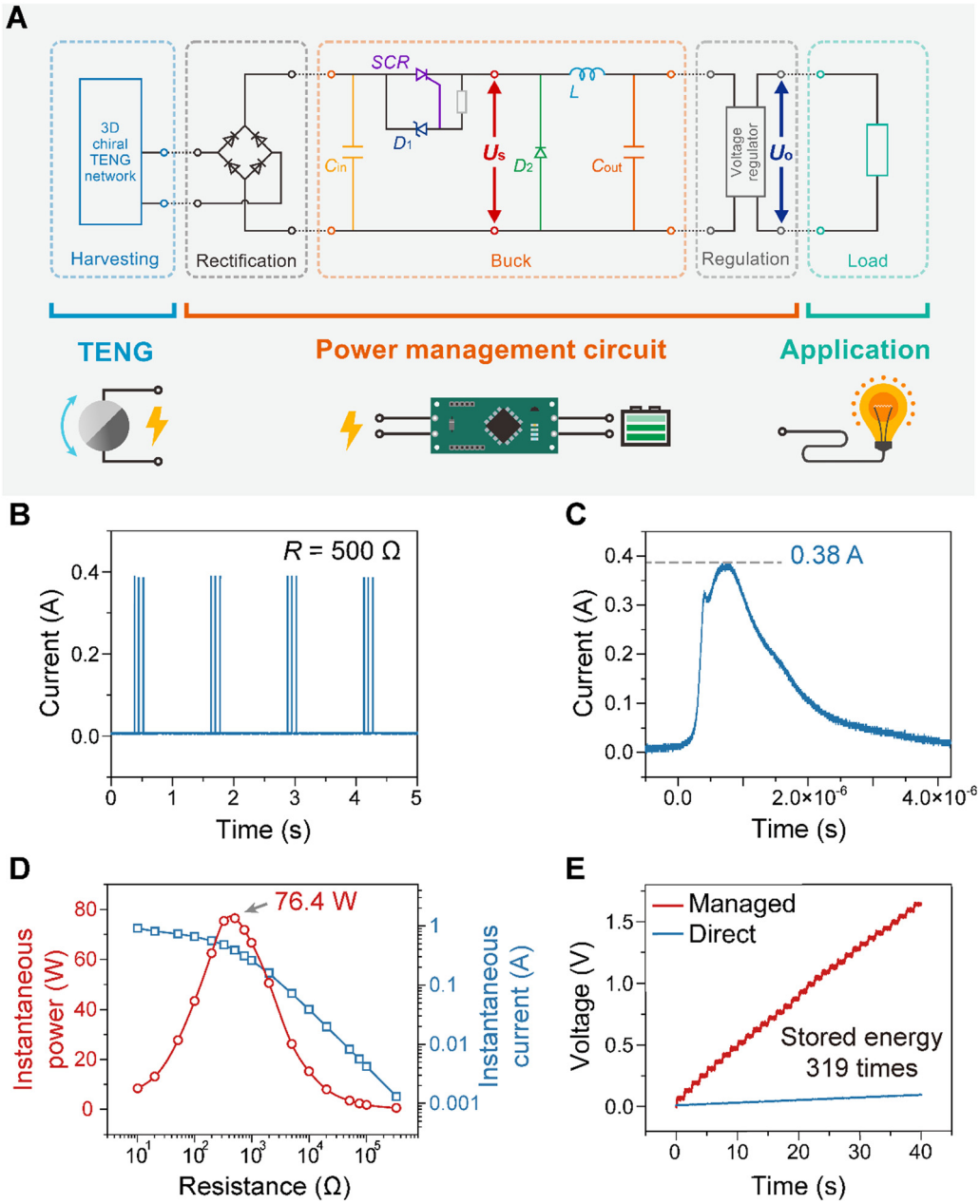

Fig. 5 Power management for the chiral network. (A) Circuit diagram of the power management circuit. (B) and (C) Output current after the switch (B) and the enlarged view (C). (D) Dependence of instantaneous current and power on different resistive loads. (E) Charging performance enhancement of the network based on power management.

clean energy as well. The inexhaustible renewable energy from waves is expected to play a crucial role in carbon neutrality in the future.

Fig. 6(B) clearly depicts the wave energy harvesting behavior of the large-scale chiral TENG network. The TENG units floating in water form a lattice-like structure as a chirally correlated network, similar to the chiral metamaterial. It can be regarded as a new metamaterial form with large sizes and water as a medium. As the water wave propagates across the network, the mechanical energy is absorbed by the network and agitates the TENG units to rotate *via* chiral coupling, which finally "dissipates" into electricity, and the wave is thus smoothed with energy loss. The lateral disturbance can also arouse TENG rotation, presenting a good omnidirectional harvesting capability. If the network is large enough, local agitations may also propagate inside the network as the wave in a material. Unlike traditional bulky and rigid machines, the 3D TENG network can distribute widely depending on the scale, which matches the distribution characteristics of water wave energy well. The flexibility of the network allows it to be more adaptive in severe ocean environments. Meanwhile, it can be expected that other exotic behaviors in the metamaterial can be transplanted to the

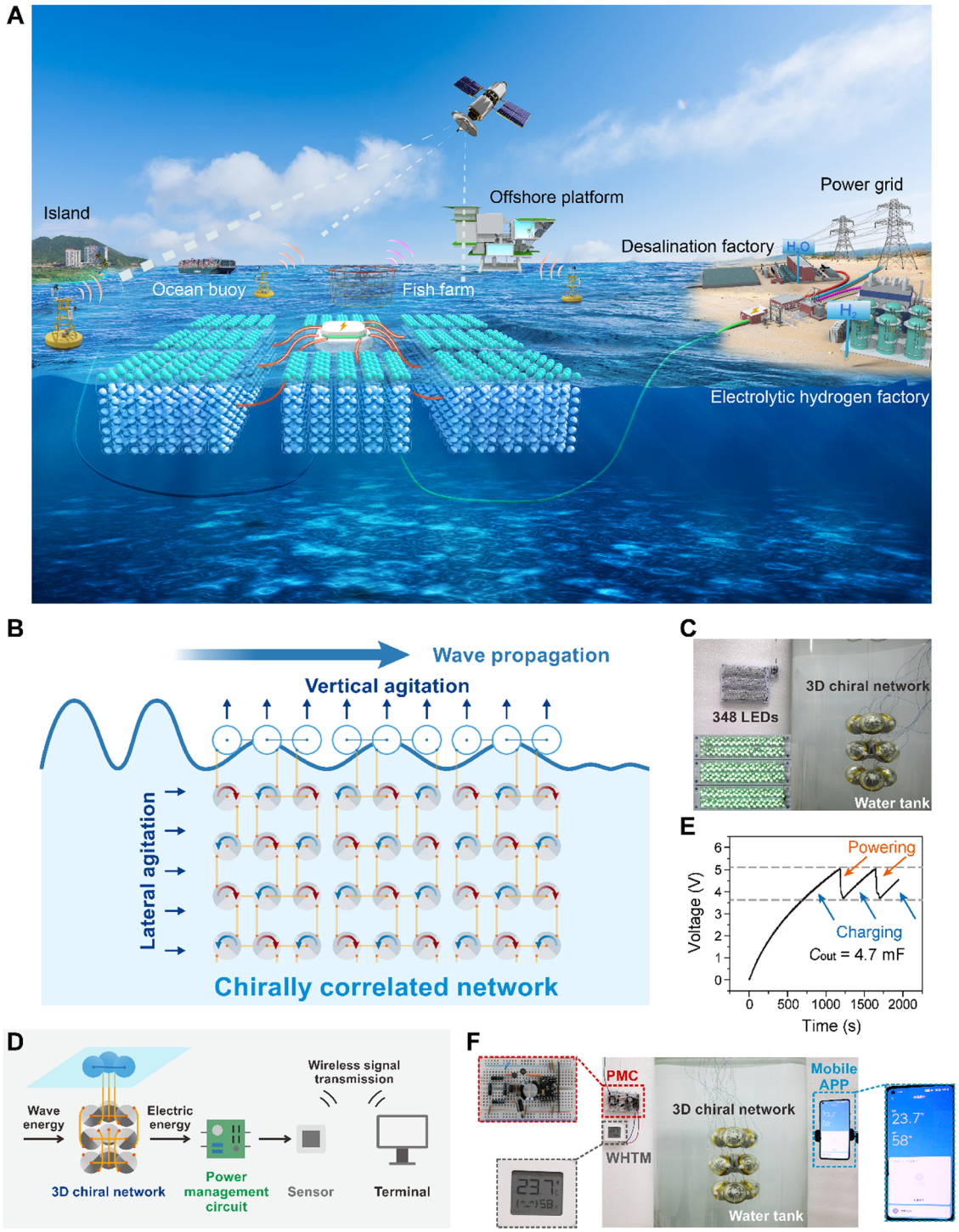

Fig. 6 Application demonstrations of the chiral network. (A) The schematic prospect of application systems based on a large-scale 3D chiral TENG network as a marine power station. (B) Schematic diagram of the wave energy harvesting behavior of the large-scale chiral TENG network. (C) Photograph of 348 LEDs powered by the 3D chiral network. (D) Schematic diagram of self-powered systems based on the network. (E) Voltage curve of the output capacitor. (F) Photograph of the 3D chiral network to power a wireless hygro-thermometer.

TENG network, providing a new paradigm for improving the performance of wave energy harvesting devices.

As an intuitive demonstration of the output performance, 348 light-emitting diodes (LEDs) can be easily lit up by the TENG network, as shown in Fig. 6(C), and Movies S4 and S5 (ESI†). An important application of the TENG network is to constitute self-powered systems, as presented in Fig. 6(D). The system typically consists of the 3D chiral network, the power management circuit, and a sensor, and the acquired data can be transmitted wirelessly to a remote terminal. The system does

not need any batteries, thus greatly reducing the cost of maintenance, especially for the situation in distant oceans. Practically, a self-powered temperature and humidity monitoring system was fabricated as a demonstration. A 4.7 mF capacitor is first charged from 0 V to 5.1 V in 1183 s before the voltage regulator is automatically switched on to supply power to a commercial wireless hygro-thermometer (WHTM). The device runs well for 32 s and sends data to the mobile phone successfully (Movie S6, ESI†). At the same time, the voltage of C_{out} decreased to 3.6 V and proceeded to the next charging cycle (Fig. 6(E) and (F)).

Conclusions

In this work, inspired by the structure of mechanical metamaterials, a novel three-dimensional chiral network of triboelectric nanogenerators is designed for the first time to effectively harvest water wave energy. Unlike traditional bulky and rigid machines, the 3D TENG network adopts a distributed architecture with chiral connections between unbalanced units, which imparts the network flexibility, hyper-elasticity in water, and wave-absorption behavior, similar to mechanical chiral metamaterials. The network can be configured to different scales and depths to harvest wave energy in all directions. Three types of networks were studied, namely serial, parallel, and hybrid, and corresponding theoretical models are established. The dependence of output on the frequency and height of waves was also investigated in detail based on a typical TENG structure with multilayer electrodes and intercalated pellets. Then, a comprehensive energy harvesting system integrated with a power management circuit was constructed, with the stored energy enhanced by about 319 times. Moreover, a self-powered sensing and signal transmission system was demonstrated. The novel 3D network shows great potential for ocean blue energy harvesting and self-powered systems based on TENGs, which can be more adaptive to severe ocean environments with flexible and distributed characteristics. The work also presents an insightful paradigm shift from mechanical metamaterial designs to energy harvesting networks, with similarities in mechanical wave energy absorption and conversion, inspiring novel energy harvesting systems and other strongly coupled machinery systems of multiple units based on metamaterials.

Experimental section

Fabrication of the TENG unit

A PET sheet was cut into thirteen transverse plates and three longitudinal plates using a laser cutter (PLS 6.75, Universal Laser Systems). Aluminum foils were attached to the PET plates, which were then spliced together into a spherical multilayer structure. The Al foils were connected together to form two independent electrodes. PTFE pellets with a diameter of 4 mm were intercalated between layers and filled about half of the spherical structure. A spherical polystyrene (PS) shell was used for encapsulation. The hemispherical mass shell was made of Sn–Bi alloy through melting and molding, and attached to one side of the spherical shell corresponding to one of the electrodes. The structures were sealed with epoxy resin for water-proofing, forming a TENG unit of about 80 mm in diameter.

Fabrication of the 3D chiral network

Four nylon holders (1.2 cm × 1.2 cm) were mounted around the periphery in the horizontal central plane of each TENG unit. Polyethylene (PE) lines (0.6 mm in diameter) were used as connection ligaments. The length of the horizontal ligaments between the chiral units of the same layer was 3 cm. In the vertical direction, the outer ligaments were 13 cm in length and the inner ligaments were 10 cm for the serial network, and they were all 13 cm for the parallel network. The floats were hollow PS spheres.

Characterization and measurement

A linear motor (Linmot) was applied to control most agitations. A wave maker (RW-20) was employed to generate lateral water flow. A rack and pinion mechanism was adopted to convert the linear motion into rotation for rocking measurements in the air. The direct output current, transferred charges and the voltage of the capacitor were tested using an electrometer (Keithley 6514). The current with the switch was measured by an oscilloscope (Tektronix MDO3104). A digital multimeter (Victor VC9808$^+$) was used for the measurement of the resistor, inductor, and capacitor. The inner diameter of the cylinder water tank was 60 cm and the height was 1.5 m. The saline water was prepared by dissolving sea salt into tap water until 3.5% salinity was achieved.

Author contributions

L. X. conceived the idea. L. X. designed the device and experiments. X. L. designed the circuit. P. L. and X. Y. fabricated the device. X. L. fabricated the network and did the experiments. X. L., L. X., H. W. and H. Q. discussed the data and prepared the figures. L. X., X. L. and Z. L. W. wrote and revised the manuscript. L. X. and Z. L. W. guided the project.

Conflicts of interest

The authors declare no competing interests.

Acknowledgements

The research was supported by the National Key R & D Project from the Minister of Science and Technology (2021YFA1201603, 2021YFA1201601), the National Natural Science Foundation of China (51605033, 51735001), and the Youth Innovation Promotion Association, CAS (2019170).

References

1 R. A. Shelby, D. R. Smith and S. Schultz, *Science*, 2001, **292**, 77–79.
2 M. Wegener, *Science*, 2013, **342**, 939–940.
3 M. Kadic, T. Buckmann, R. Schittny and M. Wegener, *Rep. Prog. Phys.*, 2013, **76**, 126501.
4 C. Coulais, E. Teomy, K. de Reus, Y. Shokef and M. van Hecke, *Nature*, 2016, **535**, 529–532.
5 L. Wu, Y. Wang, Z. Zhai, Y. Yang, D. Krishnaraju, J. Lu, F. Wu, Q. Wang and H. Jiang, *Appl. Mater. Today*, 2020, **20**, 100671.
6 B. Jenett, C. Cameron, F. Tourlomousis, A. P. Rubio, M. Ochalek and N. Gershenfeld, *Sci. Adv.*, 2020, **6**, eabc9943.
7 X. Yu, J. Zhou, H. Liang, Z. Jiang and L. Wu, *Prog. Mater. Sci.*, 2018, **94**, 114–173.
8 E. Callaway, *Nature*, 2007, **450**, 156–159.
9 J. Scruggs and P. Jacob, *Science*, 2009, **323**, 1176–1178.
10 S. Chu and A. Majumdar, *Nature*, 2012, **488**, 294–303.
11 A. Khaligh and O. C. Onar, *Energy Harvesting: Solar, Wind, and Ocean Energy Conversion Systems*, CRC Press, Boca Raton, 2009.
12 Z. L. Wang, T. Jiang and L. Xu, *Nano Energy*, 2017, **39**, 9–23.
13 A. F. D. Falcao, *Renewable Sustainable Energy*, 2010, **14**, 899–918.
14 M. J. B. Krieger, J.-B. Billeter and L. Keller, *Nature*, 2000, **406**, 992–995.
15 H. Xie, M. Sun, X. Fan, Z. Lin, W. Chen, L. Wang, L. Dong and Q. He, *Sci. Robot.*, 2019, **4**, eaav8006.
16 S. Li, R. Batra, D. Brown, H.-D. Chang, N. Ranganathan, C. Hoberman, D. Rus and H. Lipson, *Nature*, 2019, **567**, 361–365.
17 M. Rubenstein, A. Cornejo and R. Nagpal, *Science*, 2014, **345**, 795–799.
18 F. Fan, Z. Tian and Z. L. Wang, *Nano Energy*, 2012, **1**, 328–334.
19 Z. L. Wang, *Faraday Discuss.*, 2014, **176**, 447–458.
20 C. Wu, A. C. Wang, W. Ding, H. Guo and Z. L. Wang, *Adv. Energy Mater.*, 2019, **9**, 1802906.
21 C. Chen, Z. Wen, J. Shi, X. Jian, P. Li, J. T. W. Yeow and X. Sun, *Nat. Commun.*, 2020, **11**, 4143.
22 Z. L. Wang, J. Chen and L. Lin, *Energy Environ. Sci.*, 2015, **8**, 2250–2282.
23 S. Niu and Z. L. Wang, *Nano Energy*, 2015, **14**, 161–192.
24 Z. L. Wang, *Mater. Today*, 2017, **20**, 74–82.
25 J. Bae, J. Lee, S. Kim, J. Ha, B.-S. Lee, Y. Park, C. Choong, J.-B. Kim, Z. L. Wang, H.-Y. Kim, J.-J. Park and U.-I. Chung, *Nat. Commun.*, 2014, **5**, 4929.
26 R. Hinchet, H.-J. Yoon, H. Ryu, M.-K. Kim, E.-K. Choi, D.-S. Kim and S.-W. Kim, *Science*, 2019, **365**, 491–494.
27 L. Xu, Y. Pang, C. Zhang, T. Jiang, X. Chen, J. Luo, W. Tang, X. Cao and Z. L. Wang, *Nano Energy*, 2017, **31**, 351–358.
28 H. Wang, L. Xu, Y. Bai and Z. L. Wang, *Nat. Commun.*, 2020, **11**, 4203.
29 W. Xu, H. Zheng, Y. Liu, X. Zhou, C. Zhang, Y. Song, X. Deng, M. Leung, Z. Yang, R. X. Xu, Z. L. Wang, X. C. Zeng and Z. Wang, *Nature*, 2020, **578**, 392–396.
30 H. Hong, X. Yang, H. Cui, D. Zheng, H. Wen, R. Huang, L. Liu, J. Duan and Q. Tang, *Energy Environ. Sci.*, 2022, **15**, 621–632.
31 D.-M. Lee, N. Rubab, I. Hyun, W. Kang, Y.-J. Kim, M. Kang, B. O. Choi and S.-W. Kim, *Sci. Adv.*, 2022, **8**, eabl8423.
32 H. Shen, H. Lei, M. Gu, S. Miao, Z. Gao, X. Sun, L. Sun, G. Chen, H. Huang, L. Chen and Z. Wen, *Adv. Funct. Mater.*, 2022, **32**, 2204525.
33 Y. Zou, P. Tan, B. Shi, H. Ouyang, D. Jiang, Z. Liu, H. Li, M. Yu, C. Wang, X. Qu, L. Zhao, Y. Fan, Z. L. Wang and Z. Li, *Nat. Commun.*, 2019, **10**, 2695.
34 Z. L. Wang, *Nature*, 2017, **542**, 159–160.
35 X. Wang, S. Niu, Y. Yin, F. Yi, Z. You and Z. L. Wang, *Adv. Energy Mater.*, 2015, **5**, 1501467.
36 H. Wang, L. Xu and Z. L. Wang, *Nanoenergy Adv.*, 2021, **1**, 32–57.
37 L. Xu, T. Jiang, P. Lin, J. J. Shao, C. He, W. Zhong, X. Y. Chen and Z. L. Wang, *ACS Nano*, 2018, **12**, 1849–1858.
38 X. Yang, L. Xu, P. Lin, W. Zhong, Y. Bai, J. Luo, J. Chen and Z. L. Wang, *Nano Energy*, 2019, **60**, 404–412.
39 T. Frenzel, M. Kadic and M. Wegener, *Science*, 2017, **358**, 1072–1074.
40 I. Fernandez-Corbaton, C. Rockstuhl, P. Ziemke, P. Gumbsch, A. Albiez, R. Schwaiger, T. Frenzel, M. Kadic and M. Wegener, *Adv. Mater.*, 2019, **31**, 1807742.
41 Y. Bai, L. Xu, C. He, L. Zhu, X. Yang, T. Jiang, J. Nie, W. Zhong and Z. L. Wang, *Nano Energy*, 2019, **66**, 104117.
42 C. Zhang, L. He, L. Zhou, O. Yang, W. Yuan, X. Wei, Y. Liu, L. Lu, J. Wang and Z. L. Wang, *Joule*, 2021, **5**, 1613–1623.
43 C. Zhang, W. Tang, C. Han, F. Fan and Z. L. Wang, *Adv. Mater.*, 2014, **26**, 3580–3591.
44 S. Niu, X. Wang, F. Yi, Y. S. Zhou and Z. L. Wang, *Nat. Commun.*, 2015, **6**, 8975.
45 F. Xi, Y. Pang, W. Li, T. Jiang, L. Zhang, T. Guo, G. Liu, C. Zhang and Z. L. Wang, *Nano Energy*, 2017, **37**, 168–176.
46 W. Harmon, D. Bamgboje, H. Guo, T. Hu and Z. L. Wang, *Nano Energy*, 2020, **71**, 104642.
47 Y. Zi, S. Niu, J. Wang, Z. Wen, W. Tang and Z. L. Wang, *Nat. Commun.*, 2015, **6**, 8376.
48 G. Cheng, Z.-H. Lin, L. Lin, Z. Du and Z. L. Wang, *ACS Nano*, 2013, **7**, 7383–7391.

